JOURNAL OF SOLID STATE CHEMISTRY **123,** 93–99 (1996)
ARTICLE NO. 0156

Study of Xerogel–Glass Transition of CuO/SiO_2

G. Cordoba,* R. Arroyo,* J. L. G. Fierro,† and M. Viniegra*,[1]

*Departamento de Química, Universidad Autónoma Metropolitana-Iztapalapa, P.O. Box 55 534, 09340, México, D.F., Mexico; and
†Instituto de Catálisis y Petroleoquímica, CSIC, Campus UAM, Cantoblanco, 28049 Madrid, Spain

Received July 26, 1995; in revised form November 14, 1995; accepted November 16, 1995

The xerogel–glass transition of SiO_2 containing various amounts of CuO was studied by thermogravimetry, differential thermal analysis, Fourier transform infrared spectroscopy, diffuse UV–VIS–NIR reflectance, electron spin resonance spectroscopy, and X-ray photoelectron spectroscopy. The samples were prepared by the sol–gel process from tetraethoxysilane, and copper(II) acetate monohydrate. Significant structural changes were observed during the various stages of glass formation. It was concluded that copper(II) ions exist in two different enviroments, i.e., isolated and clustered. The results indicate that the former remains entrapped (doped) in the xerogel and glass, and that the clustered copper(II) ions were transformed into highly dispersed CuO by calcination. The relative amounts of these species depend on the copper(II) concentration and, except for the sample with 0.5% CuO, the amount of isolated copper(II) ions is lower than that of the clustered ions.

INTRODUCTION

The sol–gel polymerization of metal alkoxides in the presence of inorganic salts allows the formation of ceramic oxide materials that exhibit important microstructural properties (1). Composite materials containing fine metal or metal oxide particles dispersed in an amorphous oxide matrix are intersting solids for catalysis. Important efforts have been made in the past few years in order to develop catalysts with suitable on-stream stability and adequate acid–base properties. Copper containing solids are interesting catalysts for various processes among which we can mention dehydrogenation reactions (2), hydrogenolysis of aliphatic esters (3), methanol steam reforming (4), and carbon monoxide oxidation (5). The physicochemical properties of a catalyst are very much affected by the preparation methods. Generally, impregnation or (co)-precipitation is used to prepare copper catalysts, however, ion-exchange (6) and deposition–precipitation (7) methods have shown to be interesting routes since a better control of the surface composition can be exercised. The sol–gel technique offers a method for the synthesis of amorphous materials doped with copper complexes which present possibilities for new catalytic materials (8).

In this work we attempt to prepare copper–silica catalysts by the sol–gel method, since it allows one not only to better control the surface composition, but also to produce porous materials with improved thermal stability, superior homogeneity, and well-defined pore size distributions (9). In particular, this paper deals with the study of the xerogel–glass transition of silica with various amounts of copper, by means of thermal analysis and spectroscopic techniques, in order to establish the copper ions structure within the silica network, and to establish how the copper loading influences the agglomeration of surface copper species.

EXPERIMENTAL

1. Sample Preparation

Silica glasses containing 0.5, 1.0, 5.0, and 10 mol% of CuO, hereafter referred to as SCuO-0.5, SCuO-1, SCuO-5, and SCuO-10, were prepared by the sol–gel method from $Si(OC_2H_5)_4$ (TEOS) and $Cu(CH_3COO)_2 \cdot H_2O$. TEOS was first partially hydrolyzed at reflux temperature with NH_4OH as catalyst, in ethanol solution with a molar ratio of $TEOS/C_2H_5OH/H_2O/NH_4OH = 1:4:1:0.33$ and the corresponding amount of $Cu(CH_3COO)_2 \cdot H_2O$. After the solution was stirred for 10 min, 3 mol of H_2O were added, and the reflux was continued for another 50 min. The resultant mixture was aged for 24 h, and the residual liquid was then removed by decanting. The solids were converted to xerogels by heating at 353 K in a drying over for 24 h, and later divided in aliquots which were subjected to various heating processes. The samples were heated in a furnace at 473, 673, 873, and 1073 K for 72 h in air.

2. Characterization

The samples were analyzed with Fourier transform infrared spectroscopy (FTIR), diffuse UV–VIS–NIR reflectance spectroscopy, electron spin resonance (ESR) spectroscopy, thermogravimetry (TG), differential thermal

[1] To whom correspondence should be addressed.

0022-4596/96 $18.00

analysis (DTA), X-ray diffraction (XRD), and X-ray photoelectron spectroscopy (XPS).

TG and DTA measurements were performed with a Shimadzu model DT-30 analyzer in an open aluminium basket using a heating rate of 20 K/min. Fourier transform infrared transmission spectra were recorded with a Nicolet spectrometer model MX-1, using the technique of KBr pellets and working with a resolution of 2 cm^{-1}. The surface area of the samples was calculated by the Brunauer, Emmett, and Teller (BET) method from the adsorption isotherms of nitrogen at 77 K, measured in a commercial Quantasorb equipment (Quantachrome Co.) and taking a value of 0.162 nm^2 for the cross-sectional area of the adsorbed nitrogen molecule. A Cary Model 1711 diffuse reflectance accessory attached to a Cary 17-D spectrometer allowed the diffuse reflection measurements in the range 200–1200 nm, using freshly synthesized MgO samples as a reference. The samples were pressed into discs, which were positioned in the collector port. The ESR measurements were carried out in a Bruker spectrometer model 200-D SRC-A, working at 9.3 GHz (X-band) with a 100 kHz field modulation. The spectra were recorded at 77 K. The finely powdered sample, contained in a quartz tube, was introduced in the resonance cavity. The XRD patterns were obtained in a Siemens D-500 diffractometer using Cu$K\alpha$ radiation (λ = 0.1543 nm). Bragg's angles ranging from 5° to 70° were scanned at a rate of 1°/min. The XPS spectra were recorded with a Fisons ESCALAB 200R spectrometer equipped with a hemispherical electron analyzer and Mg$K\alpha$ X-ray radiation source ($h\nu$ = 1253.6 eV) powered at 12 kV and 10 mA. All samples were first outgassed in the turbo-pumped pretreatment chamber for 0.5 h before they were moved into the ion-pumped analysis chamber. The residual pressure during data acquisition was maintained below 7×10^{-9} Torr. The spectra were obtained for the samples outgassed in vacuum and for samples reduced in flowing H_2 at 473 and 523 K for 1 h. The binding energies (BE) were determined with an accuracy of ±0.2 eV. The Si 2p peak with a BE of 103.4 eV was chosen as the internal reference.

RESULTS AND DISCUSSION

Figure 1 illustrates the TG and DTA profiles obtained for the sample SCuO-10. It may be observed that the xerogel to oxide transition takes place in several steps. The thermal decomposition of the xerogel begins at room temperature with an endothermic loss of ethanol and water and continues up to 403 K (10). A second process is present and overlaps with the first weight loss. This endothermic peak has a temperature of 488 K and it is assigned to the decomposition of ammine copper complexes (11). The next stage is the decomposition of acetate groups which is strongly exothermic and begins at 518 K and ends at 623 K (12). The process continues with a smooth exothermic weight loss between 663 and 853 K. This process is assigned to the condensation of residual —OH groups with elimination of water and to the condensation of nonbonded oxygens (10, 13). Finally, a last exothermic step can be observed between 1003 and 1083 K. This process, which occurs at constant weight, is assigned to the formation of CuO (11). The total weight loss was 15.0%. These results were used to choose the temperatures at which the samples were calcined.

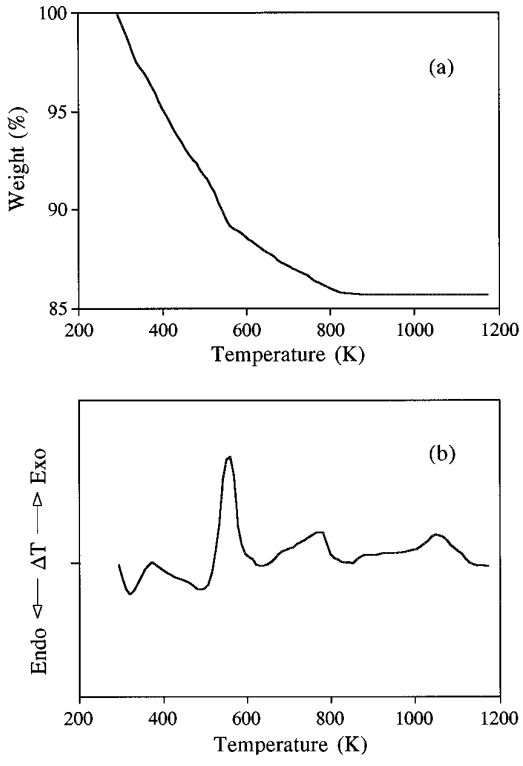

FIG. 1. Thermal analysis of SCuO-10 xerogel: (a) weight loss in air; (b) DTA performed in air.

Figure 2 shows the FTIR spectra of SCuO-10 with various thermal treatments. All the spectra show absorption bands at 1080, 800, and 460 cm^{-1}, which are assigned to different modes of Si–O–Si or O–Si–O vibrations of amorphous SiO_2 (10). The samples treated at 673 K or less show bands at 950 and 560 cm^{-1}, which are assigned to vibrations of groups with nonbonded oxygens (13). These bands disappear when the solids are treated at temperatures of 873 K or higher due to the rearrangement of the structure. The xerogel and the sample treated at 473 K also show bands 2990 and 1380 cm^{-1} corresponding to C–H vibrations (10), coming from the incomplete hydrolysis of the Si–OR groups, and from residual organic compounds. The 3450 and 1630 cm^{-1} bands are assigned to the stretching vibrations of OH species and molecular H_2O, respectively (14).

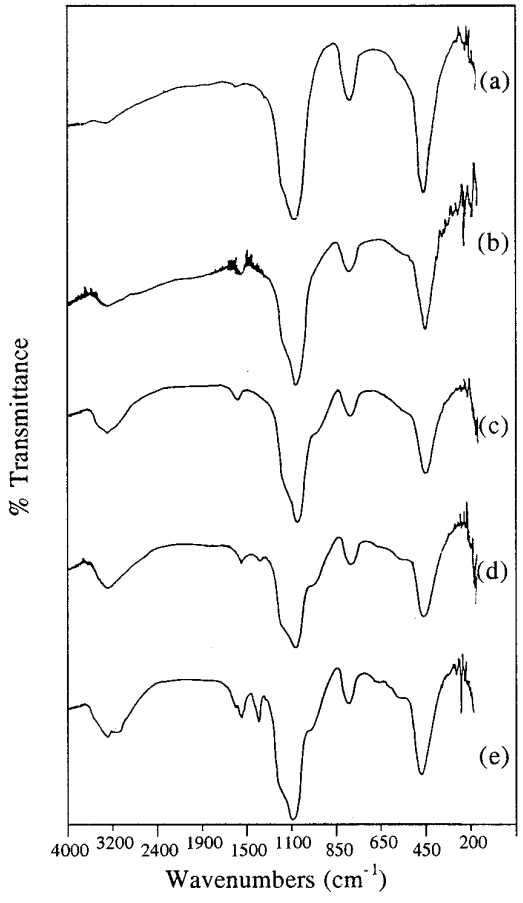

FIG. 2. FTIR spectra of SCuO-10 samples: (a) treated at 1073 K, (b) treated at 873 K, (c) treated at 673 K, (d) treated at 473 K, and (e) xerogel.

The vibrations of Cu(II)–O, that appear a 575, 500, and 460 cm^{-1} (15), cannot be observed with clarity due to the small concentration of copper(II) and because of the presence of a broad band at 460 cm^{-1} corresponding to the support. Figure 3 shows the spectra of the samples treated at 1073 K and varying copper(II) content. It may be observed that a shoulder at ca. 600 cm^{-1}, probably due to Cu(II)–O species, appears when the copper(II) content reaches a value of 10%.

UV–VIS–NIR reflectance spectra of samples with varying amount of CuO are shown in Fig. 4. These spectra correspond to the xerogels and a broad asymmetric absorption band centered near 750 nm and a sharp increase in absorption at wavelengths lower than 400 nm may be observed. The former band, present in all the samples, is assigned to *d–d* transitions of copper(II) cations and indicates the presence of copper(II) ions located in an octahedral environment (16). The increase in the amount of CuO contained in the samples induces modifications in the asymmetry and intensity of the band. At the lowest concentration tested (0.5%), the copper(II) ions seem to exist in two different environments, suggesting that different precursor species are present (11). The UV spectrum for SCuO-0.5 xerogel (Fig. 5) shows two bands at 255 and 340 nm. The first is ascribed to charge transfer between oxygen and isolated copper(II) ions and the latter to charge transfer in clustered ions (11), pointing out that the precursor species exist in two different environments.

Figure 5 shows the UV–VIS–NIR reflectance spectra of SCuO-0.5 with various thermal treatments. In comparison to the results obtained with the xerogel, the *d–d* transition band of copper(II) shifts to higher wavelengths as the calcination temperature is raised to 673 K, and this suggests the decomposition of copper(II)–ammine complexes. The bands due to charge transfer shift to higher wavelengths when the calcination temperature reaches a value of 673 K, and at higher calcination temperatures the bands present a broadening, especially that assigned to charge transfer in clusters. The 700–900 nm absorption band can be assigned to octahedral copper(II) ions incorporated in silicate glasses (17). The spectrum of the sample calcined at 1073

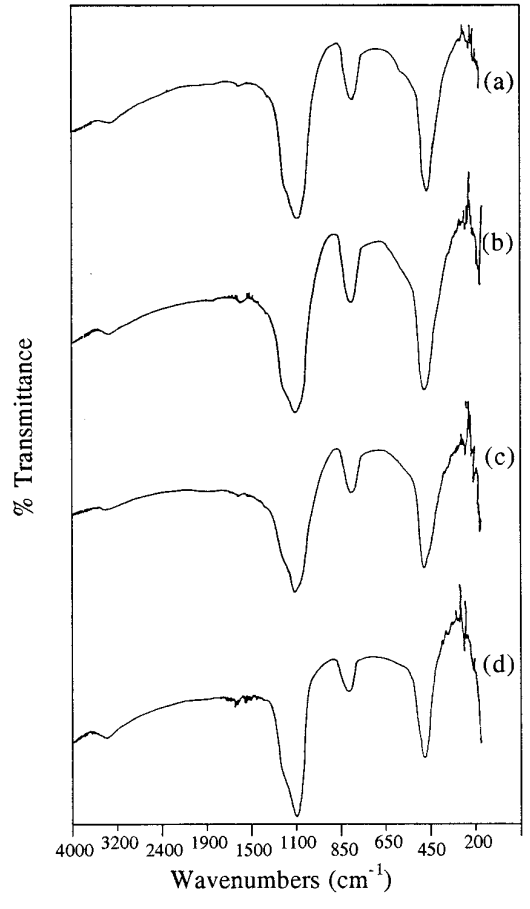

FIG. 3. FTIR spectra of the samples heated at 1073 K: (a) SCuO-10, (b) SCuO-5, (c) SCuO-1, and (d) SCuO-0.5.

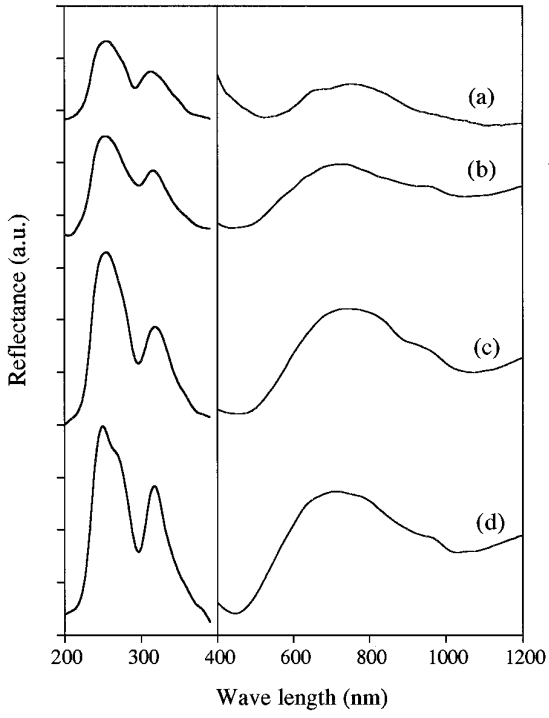

FIG. 4. Reflectance spectra in the UV–VIS–NIR spectral range of xerogels: (a) SCuO-0.5, (b) SCuO-1, (c) SCuO-5, and (d) SCuO-10.

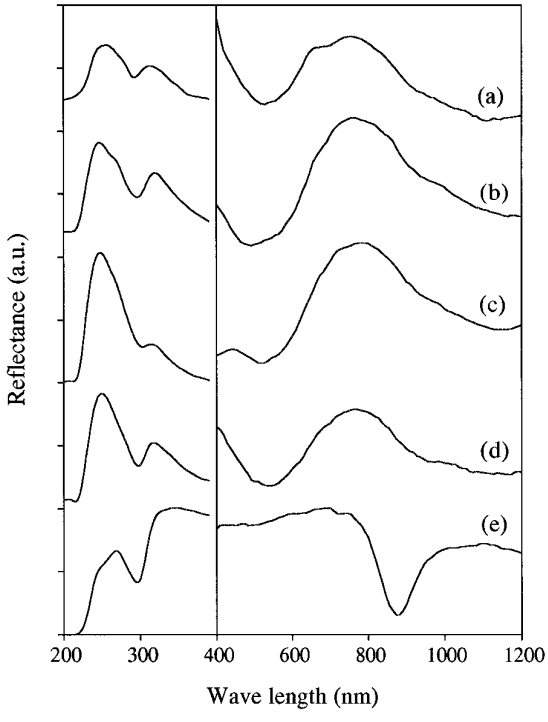

FIG. 5. Reflectance spectra in the UV–VIS–NIR spectral range of SCuO-0.5: (a) xerogel; and heated at (b) 473, (c) 673, (d) 873, and (e) 1073 K.

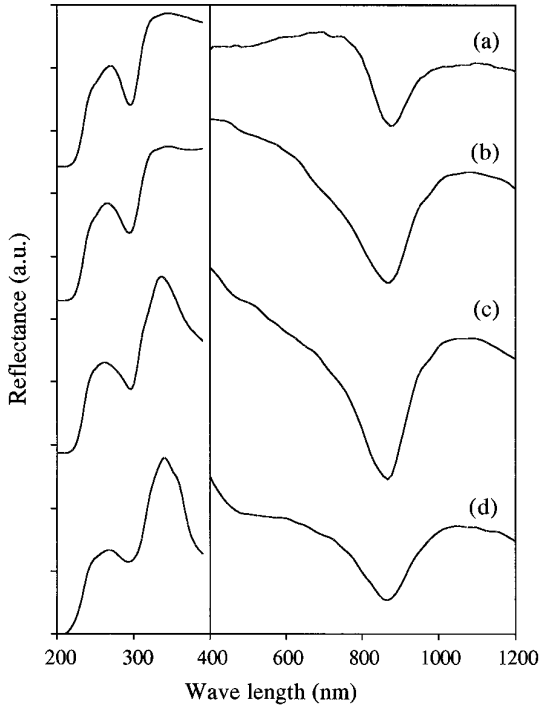

FIG. 6. Reflectance spectra in the UV–VIS–NIR spectral range of samples treated at 1073 K: (a) SCuO-0.5, (b) SCuO-1, (c) SCuO-5, and (d) SCuO-10.

K differs drastically from the others, showing a structure which is intermediate between that of the copper(II) ions and that of CuO (15). A comparison between UV–VIS–NIR spectra of samples treated at 1073 K, shown in Fig. 6, suggests that the amount of CuO clustered is greater in samples with copper loadings above 1%. This may be clearly seen through the intensity of the band located at 340 nm. The band near to 240 nm indicates the presence of isolated copper(II) ions (11) in all the samples.

These results point out the existance of two copper(II) species in all samples, one within the silica network and the other one forming clusters.

BET surface areas of the samples pretreated at 673 and 1073 K are given in Table 1. The surface areas decrease

TABLE 1
Specific Surface Area Results

Thermal treatment (K)	Samples	Surface area (m^2/g)
673	SCuO-0	104
	SCuO-5	200
	SCuO-10	214
1073	SCuO-0	65
	SCuO-5	119
	SCuO-10	129

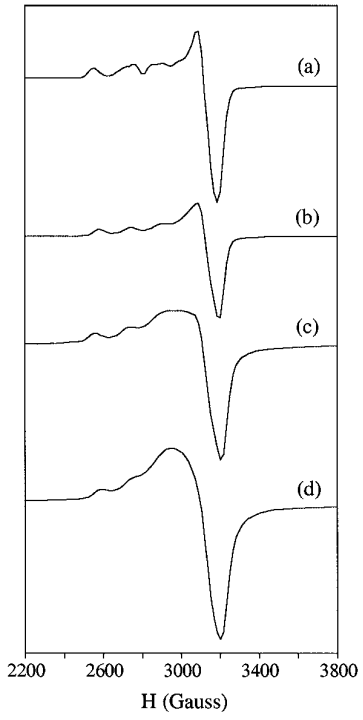

FIG. 7. ESR spectra of xerogels: (a) SCuO-0.5, (b) SCuO-1, (c) SCuO-5, and (d) SCuO-10.

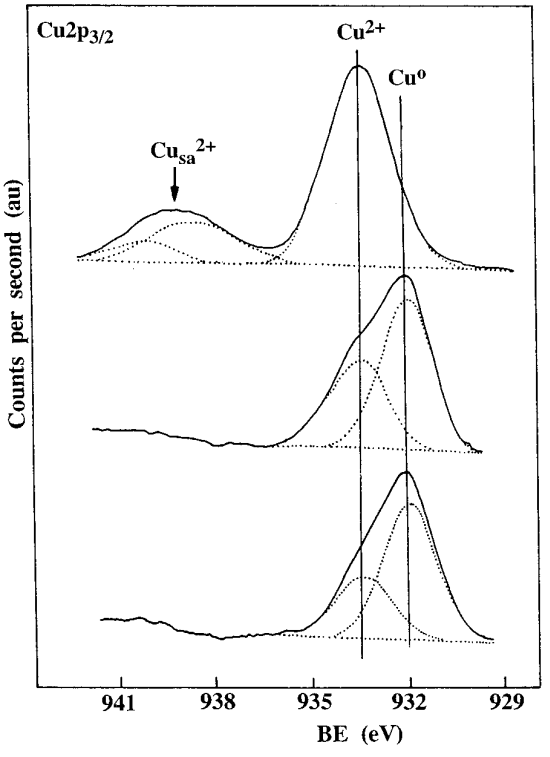

FIG. 8. XPS spectra of SCuO-5 treated at 1073 K: (top) Vacuum, (center) H_2 reduced at 473 K, and (bottom) H_2 reduced at 523 K.

with a rise in calcination temperature and increase with the addition of copper. This latter fact suggests that the copper is effectively introduced into the silica network.

The XRD patterns for all samples were indistinguishable from that of the pure SiO_2, even at 10% copper content and calcined at high temperatures. Shimokawabe *et al.* (6) obtained CuO patterns for samples prepared by ion exchange containing 8 and 10% copper and calcinated at 1073 K. Therefore, the sol–gel method stabilizes the CuO phase in a highly dispersed state.

The ESR spectra of Cu(II) ions in the various xerogels are shown in Fig. 7. These spectra are anisotropic and have hyperfine splitting (HFS) structures. The splitting patterns are not identical. The ESR spectrum of the sample SCuO-0.5 shows the structure of two types of copper(II) ions, one incorporated into the silica network (21) and the other monomolecularly dispersed over the silica surface (22). In the samples with 1% or more of CuO, the HFS is poorly resolved and the resolution is dependent on the concentration of CuO in the samples. This may be explained if we consider that at high copper loadings the average separation distance between copper(II) ions on the surface becomes so small that dipolar broadening effects prevent the observation of the $g\perp$ hyperfine components (18, 19, 22), while the cations trapped within the silica network remain in sites of larger spacing (18, 22).

Figures 8 and 9 illustrate XPS core level spectra of the

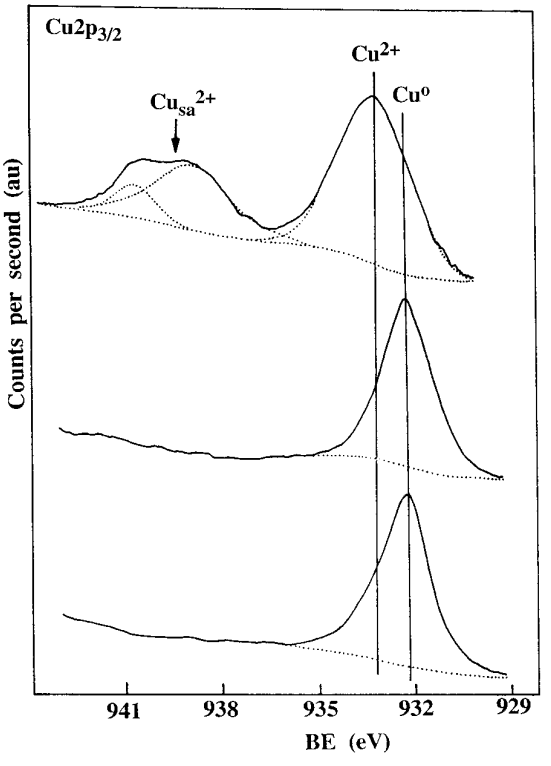

FIG. 9. XPS spectra of SCuO-10 treated at 1073 K: (top) Vacuum, (center) H_2 reduced at 473 K, and (bottom) H_2 reduced at 523 K.

TABLE 2

Binding Energies[a] (eV) of the Core Level Spectra and XPS Intensity Ratios for SCuO-5 and SCuO-10 Pretreated at 1073 K

Samples	Treated at (K)	Cu $2p_{3/2}$	I_{Cu}/I_{Si}
SCuO-5	295 (vacuum)	933.5	0.0506
	473 (reduction)	933.6 (41)	0.0393
		932.0 (59)	
	523 (reduction)	933.6 (36)	0.0383
		932.2 (64)	
SCuO-10	295 (vacuum)	935.6 (13)	0.226
		933.5 (87)	
	473 (reduction)	932.2	0.163
	523 (reduction)	932.2	0.155

[a] The Si2*p* peak with a BE of 103.4 eV was chosen as the internal reference.

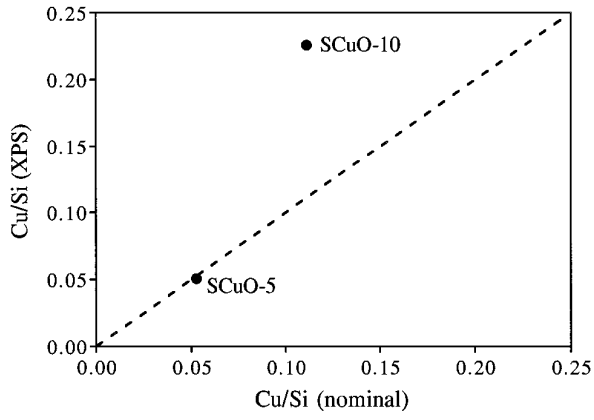

FIG. 10. XPS composition vs nominal composition of SCuO-5 and SCuO-10 samples.

samples SCuO-5 and SCuO-10, respectively, calcined at 1073 K, and the binding energies of the more intense peaks are shown in Table 2. The SCuO-5 sample outgassed under vaccum presents only the peak corresponding to oxidized copper(II) species (20); nevertheless the presence of a small amount of copper(I) may not be excluded since the shake-up satellite line, located about 9 eV above the principal line, presents scarce intensity. Metallic copper appears when the sample is reduced at 473 and 520 K, with a concomitant decrease in the I_{Cu}/I_{Si} ratio due to the aggregation of copper into small particles.

The SCuO-10 sample shows a somewhat different behavior. The sample outgassed presents two contrbutions to the Cu 2*p* peak, one of high BE probably due to the interaction of copper(II) with the silicate network and the other at lower BE, associated with CuO. This sample is completely reduced at 473 K. These spectra show the reduction of surface copper species, and therefore, we are not able to observe the copper species entrapped in the bulk. Despite the sintering of copper particles due to the reduction process, the Cu/Si ratio is reasonably good. Figure 10 shows the surface composition (by XPS) plotted against the bulk (nominal) composition for the SCuO-5 and SCuO-10 samples. It may be observed that at 5% copper loading, the solid is homogeneous, while at 10% copper content the surface is enriched with copper.

CONCLUSIONS

SiO_2 samples containing various amounts of CuO prepared by the sol–gel method were characterized by various techniques. It was found that the copper(II) ions exist in two different environments in the samples, one isolated copper(II) species incorporated into the silica network and the other clustered on the silica surface. The spectroscopic results showed that for samples where the amount of CuO is 1% or lower the copper(II) ions trapped in the surface are monomolecularly dispersed, and for the samples with copper loadings above 1%, small aggregates that are highly dispersed are formed. The XPS results showed that after reduction by hydrogen the copper(II) ions located at the surface were reduced and aggregated to form small copper particles. Despite the high calcination temperature used, the surface areas of the samples are reasonably good, and the copper oxide remains in a highly dispersed state.

REFERENCES

1. A. M. Buckley and M. Greenblatt, *J. Non-Cryst. Solids* **146,** 97 (1992).
2. R. Pearce and W. R. Patterson, ''Catalysis and Chemical Processes.'' p. 274. Leonard Hill, Glasgow, 1981.
3. J. W. Evans, P. S. Casey, M. S. Wainwright, D. Y. Trimm, and N. W. Cant, *Appl. Catal.* **7,** 31 (1983).
4. K. Takahashi, N. Takezawa, and H. Kobayashi, *Appl. Catal.* **2,** 363 (1982).
5. Y. F. Yu Yao and J. T. Kummeer, *J. Catal.* **46,** 388 (1977).
6. M. Shimokawabe, N. Tekezawa, and H. Kobayashi, *Appl. Catal.* **2,** 379 (1982).
7. Ch. Sivaraj and P. Kantarao, *Appl. Catal.* **45,** 1103 (1988).
8. J. Yan, A. M. Buckley, and M. Greenblatt, *J. Non-Cryst. Solids* **180,** 180 (1995).
9. C. J. Brinker and G. W. Scherer, ''Sol–Gel Science. The Physics and Chemistry of Sol–Gel Processing.'' Academic Press, San Diego, 1990.
10. Z. Congshen, H. Lisong, G. Fuxi, and J. Zhonghong, *J. Non-Cryst. Solids* **63,** 105 (1984).
11. M. Shimokawabe, H. Asakawa, and N. Takezawa, *Appl. Catal.* **59,** 45 (1990).
12. S. Doeuff, M. Henry, and C. Sanchez, *in* ''Better Ceramics Through Chemistry II'' (C. J. Brinker *et al.*, Eds.), p. 653. Elsevier Science, New York, 1986.
13. N. Tohge, G. S. Moore, and J. D. Mackenzie, *J. Non-Cryst. Solids* **63,** 95 (1984).
14. K. Nakamoto, ''Infrared and Raman Spectra of Inorganic and Coordination Compounds,'' 4nd ed., p. 228. Wiley–Interscience, New York, 1986.
15. B. Orel, F. Svegl, N. Bukovec, and M. Kosec, *J. Non-Cryst. Solids* **159,** 49 (1994).

16. B. S. Bae and M. C. Weinberg, *J. Non-Crys. Solids* **168,** 223 (1994).
17. A. Duran and J. M. Fernandez Navarro, *Phys. Chem. Glasses* **26,** 126 (1985).
18. W. Weng, J. Yang, and Z. Ding, *J. Non-Cryst. Solids* **170,** 134 (1994).
19. A. Carrington and A. D. MaLachlan, ''Introduction to Magnetic Resonance,'' p. 171. Harper & Row, New York, 1969.
20. A. Guerrero-Ruiz, I. Rodríguez-Ramos, G. J. Siri, and J. L. G. Fierro, *Surf. Interface Anal.* **19,** 548 (1992).
21. S. Dave and R. K. Maccrone, ''Better Ceramics Throuh Chemistry II'' (C. J. Brinker *et al*., Eds.), p. 605. Elsevier Science, New York, 1986.
22. S. Ikoma, S. Takano, E. Nomoto, and H. Yokoi, *J. Non-Crys. Solids* **13,** 130 (1989).